Measurement Sensitivity and Estimation Error in Distribution System State Estimation using Augmented Complex Kalman Filter

Alan Louis, *Member*, *IEEE*, Gerard Ledwich, *Senior Member*, *IEEE*, Geoff Walker, *Member*, *IEEE*, and Yateendra Mishra, *Member*, *IEEE*

***Abstract*—Distribution state estimation (DSE) is an essential part of an active distribution network with high level of distributed energy resources. The challenges of accurate DSE with limited measurement data is a well-known problem. In practice, the operation and usability of DSE depend on not only the estimation accuracy but also the ability to predict error variance. This paper investigates the application of error covariance in DSE by using the augmented complex Kalman filter (ACKF). The Kalman filter method inherently provides state error covariance prediction. It can be utilized to accurately infer the error covariance of other parameters and provide a method to determine optimal measurement locations based on the sensitivity of error covariance to measurement noise covariance. This paper also proposes a generalized formulation of ACKF to allow scalar measurements to be incorporated into the complex-valued estimator. The proposed method is simulated by using modified IEEE 34-bus and IEEE 123-bus test feeders, and randomly generates the load data of complex-valued Wiener process. The ACKF method is compared with an equivalent formulation using the traditional weighted least squares (WLS) method and iterated extended Kalman filter (IEKF) method, which shows improved accuracy and computation performance.**

***Index Terms*—Augmented complex Kalman filter, direct load flow, distribution system state estimation, error variance, sensitivity analysis.**

I. Introduction

DISTRIBUTION state estimation (DSE) is considered an important part of an operation of a distribution network with high level of distributed energy resources (DERs). The increasing penetration of DERs requires a shift towards active distribution networks with smarter and more advanced monitoring tools to improve network planning and operation. The purpose of state estimation is to determine the most probable state of the system based on the measured quantities. While the deployment of phasor measurement units (PMUs) to improve the observability are common in transmission networks, distribution networks have more significant challenges with state estimation due to the limited real-time information and the network topology. Radial distribution networks can be far-reaching, extending into remote areas. Since the measurement equipment and infrastructure are typically expensive, it is essential to determine the minimal number of sensors in the optimal locations to satisfy the observability.

The classic approach to state estimation is based on the weighted least squares (WLS) method, which determines the best estimate of static state using the weighted sum of the square of error [1]-[4]. In practical applications, this is formulated as an over-determined system of nonlinear equations and solved as WLS problems [5]. In recent years, there have been developments in the implementation of WLS, particularly around the linearization of the measurement function and improving the robustness of convergences [6]-[9]. The typical WLS methodology is considered as a static approach to power system state estimation, which means that estimates are extracted from a single snapshot of measurements. State estimates from previous time steps are not considered in the estimate of current state since state transition is ignored [10]-[12]. This has led to the development of dynamic state estimators. More recently, methods based on the Kalman filter (KF) framework have been proposed and developed. The formulation of WLS and KF methods are similar in that process and measurement noise covariances are used to provide the best guess state estimate. However, KF is a recursive estimator that is considered as a dynamic approach to state estimation, compared with the snapshot approach of classical WLS [12].

There are two paradigms in power system dynamic state estimation, which differ in terms of the studied dynamics and time scales. One paradigm, typically referred to as forecasting-aided state estimation (FASE) or tracking state estimators (TSE), considers the progression of quasi-steady states of the power system, i. e., the slow evolution of the static state. In another paradigm, full system dynamics are considered in terms of classic dynamic models such as generator rotor angles [10]-[15]. In this paper, the research is focused on the former paradigm.

The use of various KF frameworks in quasi-steady state

Manuscript received: March 31, 2020; accepted: May 9, 2020. Date of Cross-Check: May 9, 2020. Date of online publication: July 9, 2020.

A. Louis (corresponding author), G. Ledwich, G. Walker, and Y. Mishra are with the Queensland University of Technology, Brisbane, Australia (e-mail: a. louis@hdr. qut. edu. au; g. ledwich@qut. edu. au; geoffrey. walker@qut. edu. au; yateendra.mishra@qut.edu.au).

DOI: 10.35833/MPCE.2019.000160

estimation has been proposed. An extended KF (EKF) using a power flow based dynamic model and load forecasts are investigated in [16]. This is developed further by using the iterated KF (IKF) to estimate the full state vector with both real and reactive measurements [17]. The WLS and EKF methods are compared and the importance of the process and measurement error covariance matrices is demonstrated [18]. The EKF is used to overcome the practical issues of missing measurements caused by data dropouts [19]. A procedure for integrating PMU with the IKF is developed and the sensitivity analysis as a function of measurement and process covariance matrices is performed [20]. There have also been various applications of the unscented KF (UKF) in DSE applications. UKF is proposed to achieve better accuracy and more straightforward implementation over the classical EKF [21]. A robust UKF is proposed to handle the unknown statistics of system process and measurement noise that could bias the state estimates [22]. In general, KF methods are based on the nonlinear formulations of the measurement function. However, the challenges of these formulations have driven the need to consider linearization methods [15], [23] and derivative-free methods [24], [25]. The effectiveness of these methods depends on the nonlinearity of the dynamic system and whether the derivatives of nonlinear equations can be calculated [12].

A linear approach to state estimation is considered by integrating the direct load flow method in the previous work. A DSE using the augmented complex KF (ACKF) and the direct load flow method is developed as a new approach to quasi-steady state estimation. The approach also allows the network to be divided into sub-layers so that the network can be processed more efficiently [26]. The typical approach for DSE is to separate magnitude and phasor angle in the state vector, whereas complex-valued estimators consider the state as a vector of complex values. ACKF has been proposed in other applications such as frequency estimation in power networks [14].

A gap of complex-valued estimators in the previous work considers how scalar measurements can be incorporated in the augmented complex form. Complex-valued measurements such as PMU are not as commonly available in distribution networks as scalar measurements such as voltage magnitude or branch currents. The application of complex-valued estimators should consider how both complex-values and scalar measurements can be integrated without bypassing second-order statistics. In DSE applications, the available measurements are expected to be limited. The DSE algorithm should provide the best guess estimate of the network state with limited measurement and an accurate estimate of the error variance. The accuracy is a crucial aspect that defines the usability of the DSE. However, determining and validating the accuracy of estimation is not inherent in many DSE techniques. While there have been significant advancements in DSE, the prediction and validation of estimation error within DSE techniques are not well researched.

This research is an extension of the previous work on ACKF DSE. This paper demonstrates the use of error covariance of the state estimate to determine the error covariance of other linearly related network parameters. Furthermore, the Ricatti equations can be used to calculate the sensitivity of the estimation to measurement types and locations. Therefore, a method is provided to determine optimal measurement points that improve overall estimation accuracy. Traditionally, this is difficult to determine because different measurement types provide improvements to different areas of estimations. For example, the influence of an additional bus voltage magnitude measurement on power flow estimation accuracy is not well understood.

The contributions of this paper are as follows:

1) Define a generalized form of the observation model for ACKF DSE to incorporate scalar or complex-valued measurements of bus injection current, branch injection current, or bus voltage.

2) Derive the relationship between the *a posteriori* error covariance of the state estimate and other linearly related variables, to allow the estimation of error across multiple network parameters.

3) Provide a method for sensitivity analysis of the Riccati update equation of the state error covariance, to calculate changes in error covariance due to additional measurement locations.

Simulations with a modified IEEE 34-bus and IEEE 123-bus test feeders are used to verify the proposed work. The network load data is randomly generated to remove any influence of covariances in data that could be exploited in the estimation technique. It is understood that the relationships in the data are often used as pseudo-measurements to improve the accuracy of DSE instead of real-time measurements. This paper does not exclude the use of pseudo-measurements to improve the estimation. However, the proposed methodology focuses on a limited set of simulated measurements to demonstrate the performance in the estimation of error variance.

The rest of the paper is organized as follows. Section II discusses the background of the ACKF DSE and its formulation. Section III proposes the generalized form of the observation model. Section IV discusses how error covariance of the state estimate can be used to ascertain error covariances of other linearly related parameters, and also presents the formulation of the sensitivity of error covariance. Section V discusses the simulation methodology. Section VI discusses the simulation and test results. Section VII draws the conclusions.

II. Background

An augmented complex-valued KF is firstly introduced in [27] as a means to process general complex-valued nonlinear and nonstationary signals and bivariate signals with strong correlations. There is strong applicability in three-phase distribution networks due to the complex-valued nature of power systems, and the nonstationary nature of loads. DSE using ACKF is firstly proposed in [26]. The estimator solves the load flow by using a linear approach. This is different from the previous DSE using IKF or EKF methods which are based on nonlinear process models [16]-[18], [22].

The advantage of using the ACKF for estimation com-

pared with classical state estimation approaches is that ACKF is a recursive estimator that considers the state as complex values.

The ACKF method is derived by using the augmented states and augmented covariance matrix. A general state-space model is given as:

$$\begin{cases} \boldsymbol{x}_{k+1} = \boldsymbol{F}_{k+1}\boldsymbol{x}_k + \boldsymbol{\omega}_k \\ \boldsymbol{y}_k = \boldsymbol{H}_k\boldsymbol{x}_k + \boldsymbol{v}_k \end{cases} \tag{1}$$

where $\boldsymbol{x}_{k+1}$ is the complex state vector at the next time step $k+1$; $\boldsymbol{x}_k$ and $\boldsymbol{y}_k$ are the complex state and measurement vectors at the time step k, respectively; $\boldsymbol{F}_{k+1}$ is the transition vector at the next time step $k+1$; $\boldsymbol{H}_k$ is the measurement vector at the time step k; and $\boldsymbol{\omega}_k$ and $\boldsymbol{v}_k$ are the independent and zero-mean complex-valued Gaussian noise processes with covariance matrices $\boldsymbol{Q}_k$ and $\boldsymbol{R}_k$, respectively. From (1), the augmented state-space model can be written as:

$$\begin{cases} \boldsymbol{x}^a_{k+1} = \boldsymbol{F}^a_{k+1}\boldsymbol{x}^a_k + \boldsymbol{\omega}^a_k \\ \boldsymbol{y}^a_k = \boldsymbol{H}^a_k\boldsymbol{x}^a_k + \boldsymbol{v}^a_k \end{cases} \tag{2}$$

where $\boldsymbol{x}^a_k = \begin{bmatrix} \boldsymbol{x}_k \\ \boldsymbol{x}^*_k \end{bmatrix}$; $\boldsymbol{y}^a_k = \begin{bmatrix} \boldsymbol{y}_k \\ \boldsymbol{y}^*_k \end{bmatrix}$; $\boldsymbol{F}^a_k = \begin{bmatrix} \boldsymbol{F}_k & \boldsymbol{0} \\ \boldsymbol{0} & \boldsymbol{F}^*_k \end{bmatrix}$; $\boldsymbol{H}^a_k = \begin{bmatrix} \boldsymbol{H}_k & \boldsymbol{0} \\ \boldsymbol{0} & \boldsymbol{H}^*_k \end{bmatrix}$; $\boldsymbol{\omega}^a_k = \begin{bmatrix} \boldsymbol{\omega}_k \\ \boldsymbol{\omega}^*_k \end{bmatrix}$; and $\boldsymbol{v}^a_k = \begin{bmatrix} \boldsymbol{v}_k \\ \boldsymbol{v}^*_k \end{bmatrix}$. The superscript * represents the complex conjugate and the superscript a denotes the augmented complex form to account for complex statistics.

The use of complex statistics is not a new concept within distribution system analysis [28], [29], and has been incorporated in load forecasting models and state estimation.

A. State Model

In typical power system state estimators, the state is a vector of voltage phasor angles and magnitudes for all busses in the network. This estimator considers the state vector as a complex-valued current injection at each bus:

$$\hat{\boldsymbol{x}} = \begin{bmatrix} i_1\angle\delta_1 & i_2\angle\delta_2 & \dots & i_N\angle\delta_N \end{bmatrix}^{\mathrm{T}} \tag{3}$$

There are examples of current-based formulations of the state estimator [30]. However, the real and imaginary components are usually separated in the state vector. The formulation of a complex-valued state vector is possible using the augmented complex methodology.

The KF is a recursive estimator, where $\hat{\boldsymbol{x}}_{ij}$ is the estimate of $\boldsymbol{x}$ at time i, given observations at time $j \le i$. The transition matrix $\boldsymbol{F}$ considers the changes of state from the time step k to the next time step $k+1$.

The development of various state models for the KF is presented in [16], [17]. The transition matrix incorporates the Jacobian of the network to calculate changes in state, due to the nonlinear relation between voltage and power flows. The direct load flow approach is based on the linear relationship between bus voltage, bus injection current, and network impedance.

The previous work analyzes the measurements of network load and shows that the change in bus currents between two successive time steps, i.e., $k \to k+1$, could be characterized as white noise [26]. This assumes that the state of the network is inherently static, and any changes in bus current injections are random and indistinguishable to white noise between the successive time steps. The analysis of load data also includes a low-level penetration of solar photovoltaics. $\boldsymbol{F}$ is replaced by the identity matrix. This is consistent with the previous research on stochastic load models, which regard to actual loads like a normal distribution random variable with a stochastic perturbation of a fixed value and a white noise process normally distributed with zero mean [31], [32]. One disadvantage is that the normal load model does not categorize the switched nature of loads, nor for higher penetrations of DERs.

B. Measurement and Output Model

The measurement matrix $\boldsymbol{H}$ is formulated from the equations of the direct load flow approach. The benefit of this approach is that the output variables, voltage and branch current, are a linear function of the bus injection current, based on the $\boldsymbol{DLF} = \boldsymbol{BCBV} \cdot \boldsymbol{BIBC}$, branch-current to bus-voltage $\boldsymbol{BCBV}$, and bus-injection to branch-current $\boldsymbol{BIBC}$ matrices [33]. $\boldsymbol{BIBC}$ provides the relationship between bus current injection and branch current. $\boldsymbol{BCBV}$ provides the relationship between branch current and bus voltage. Both these matrices form the topology of the network in the direct load flow approach to allow a linear calculation of the network state.

The voltage at each bus is given by (4). The branch current is given by (5).

$$\boldsymbol{v} = \boldsymbol{v}_1 - \boldsymbol{DLF} \cdot \boldsymbol{i}_{inj} \quad \boldsymbol{DLF} \in \mathbb{C}^{n\times n} \tag{4}$$

$$\boldsymbol{i}_{branch} = \boldsymbol{BIBC} \cdot \boldsymbol{i}_{inj} \quad \boldsymbol{BIBC} \in \mathbb{R}^{n\times n} \tag{5}$$

where $\boldsymbol{v}_1$ is the source voltage; $\boldsymbol{i}_{inj}$ is the bus injection current; and n is the number of buses. Based on (4) and (5), the output matrix $\boldsymbol{y}$ can be written as:

$$\boldsymbol{y} = \begin{bmatrix} \boldsymbol{i}_{inj} \\ \boldsymbol{i}_{branch} \\ \boldsymbol{v} \end{bmatrix} = \begin{bmatrix} \boldsymbol{I} & \boldsymbol{0} & \boldsymbol{0} \\ \boldsymbol{0} & \boldsymbol{BIBC} & \boldsymbol{0} \\ \boldsymbol{0} & \boldsymbol{0} & -\boldsymbol{DLF} \end{bmatrix} \begin{bmatrix} \boldsymbol{i}_{inj} \\ \boldsymbol{i}_{inj} \\ \boldsymbol{i}_{inj} \end{bmatrix} + \begin{bmatrix} \boldsymbol{0} \\ \boldsymbol{0} \\ \boldsymbol{v}_1 \end{bmatrix} = \boldsymbol{H}\boldsymbol{x} + \boldsymbol{v}_1 \tag{6}$$

where $\boldsymbol{y}$ is a $d \times 1$ vector consisting of actual or pseudo measurements of bus injection current, branch flow or voltage, and d is the total number measurement points. Section III provides an in-depth formulation of $\boldsymbol{H}$. The methodology also allows the reconfiguration of the network topology without resetting state variables if the load identities are maintained. Since the state propagation model is the identity matrix, the state variables essentially track the load progression in the system.

C. ACKF DSE

The process for the ACKF DSE in discrete steps is as follows, and the variable descriptions for (7)-(12) can be found in [27].

1) Propagate the state estimate

$$\hat{\boldsymbol{x}}^a_{k|k-1} = \hat{\boldsymbol{x}}^a_{k-1|k-1} \tag{7}$$

2) Propagate and estimate the error covariance

$$\boldsymbol{P}_{k|k-1} = \boldsymbol{P}_{k-1} + \boldsymbol{Q}^a_{k-1} \tag{8}$$

3) Calculate the Kalman gain

$$\boldsymbol{G}^a_k = \boldsymbol{P}_{k|k-1}\boldsymbol{H}^{aH}_{k+1}\left(\boldsymbol{H}^a_{k+1}\boldsymbol{P}_{k|k-1}\boldsymbol{H}^{aH}_{k+1} + \boldsymbol{R}^a_k\right)^{-1} \tag{9}$$

4) Update the state matrix

$$\hat{\boldsymbol{x}}_{k+1}^{a}=\hat{\boldsymbol{x}}_{k}^{a}+\boldsymbol{G}_{k}\left(\boldsymbol{y}_{k}^{a}-\boldsymbol{H}_{k}^{a}\hat{\boldsymbol{x}}_{k}^{a}\right) \tag{10}$$

5) Update error covariance

$$\boldsymbol{P}_{k|k}=\left(\boldsymbol{I}-\boldsymbol{G}_{k}\boldsymbol{H}_{k}^{a}\right)\boldsymbol{P}_{k|k-1} \tag{11}$$

6) Initialize the algorithm

$$\hat{\boldsymbol{x}}_{0}^{a}=E\left(\boldsymbol{x}_{0}^{a}\right) \tag{12}$$

$\boldsymbol{H}$ is formulated based on the measurement points and the corresponding rows of ***DLF*** and ***BIBC***. In most cases, $\boldsymbol{H}$ is not expected to vary at each discrete time step, i.e., $\boldsymbol{H}^{a}=\boldsymbol{H}_{k}^{a}=\boldsymbol{H}_{k+1}^{a}$. Similarly, with the state and error covariance matrices $\boldsymbol{Q}$ and $\boldsymbol{R}$, $\boldsymbol{R}$ is defined based on the expected error covariance of the measurement points.

The measurement noise is assumed to be a Gaussian distribution with zero mean and variance σ_i^2. More accurate measurements, i.e., sensors, have lower variance, whereas less accurate measurements, i.e., pseudo, have higher variance. In $\boldsymbol{R}$, the elements are assumed to be uncorrelated [17], [30], which means the off-diagonal elements are zero and $R_{ii}=\sigma_i^2$ as the variance of the i^{th} measurement. The augmented form of $\boldsymbol{R}$ becomes $\boldsymbol{R}^{a}=\begin{bmatrix}\boldsymbol{R} & \boldsymbol{0}\\ \boldsymbol{0} & \boldsymbol{R}^{*}\end{bmatrix}$.

III. Integrating Measurement Types in Augmented Form

The use of augmented complex statistics allows the consideration of complex values, rather than separation of phasor magnitude and angles. Since the algorithm is based on the direct load flow approach, measurements are a linear calculation of network states, which means the angles of the bus injection current and bus voltage are referenced to the source bus. This approach means the data from PMU can be integrated directly into the estimator. For other measurement types such as voltage magnitude, current magnitude, or branch power flow, an additional process is needed to incorporate the data. In this section, we consider how both complex and real-valued measurements can be integrated into the estimator.

The algorithm uses the augmented complex form of $\boldsymbol{H}$, which is comprised of the selected rows of ***BIBC*** and ***DLF***. Regarding the inclusion of bus injection currents, measured or as pseudo-measurements, only the identity matrix is needed. $\boldsymbol{H}$ is of size $n\times m$, where m is the total number of measurement points. The basic formulation of $\boldsymbol{H}$ for complex-valued measurements is defined in Appendix A.

This paper proposes a generalized form of $\boldsymbol{H}$ to allow a range of measurement types to be incorporated into the augmented form. This provides flexibility in the formulation of $\boldsymbol{H}$ to handle all likely forms of distribution network measurements, whether the measurements are scalar-valued, i.e., bus voltage magnitude, or complex-valued, i.e., PMU data.

The augmented complex form inherently allows complex values to be considered. However, for scalar measurements, an alternative derivation is needed to ensure that complex statistics are maintained. A simple approach is proposed, which adopt $\mathrm{Re}(z)=\left(z-z^{*}\right)/2$ to allow a simple formulation of $\boldsymbol{H}$ and consider scalar values. We need to consider that there is a difference between the real component of measurement z and the absolute component of z, which depends on the argument φ.

For magnitude measurements, φ is unknown but is estimated by the ACKF. A compensation is introduced to correct the measurement model output:

$$\left|z_{k}\right|=\frac{\mathrm{Re}\left(z_{k}\right)}{\cos\hat{\varphi}_{k-1}} \tag{13}$$

where $\hat{\varphi}_{k-1}$ is the estimated argument of measurement z at the previous time step.

In practice, the most common form of magnitude measurements is bus voltage measurements along a distribution feeder. Typically, we would expect a minimal voltage phase angle shift along a distribution feeder, which means the compensator factor would be close to 1, i.e., $\mathrm{Re}(z)\approx|z|$.

A generalized form of $\boldsymbol{H}$ which considers scalar or complex-valued measurements is derived as:

$$\boldsymbol{H}^{a}=\begin{bmatrix}\boldsymbol{H}_{11} & \boldsymbol{H}_{12}\\ \boldsymbol{H}_{21} & \boldsymbol{H}_{22}\end{bmatrix} \tag{14}$$

Equations (15) to (22) define the formulation of $\boldsymbol{H}$.

$$\boldsymbol{H}_{11,i}=\begin{cases}\boldsymbol{I}_{i} & I_{meas,i}\in\mathbb{C}\\ \dfrac{\boldsymbol{I}_{i}}{2} & I_{meas,i}\in\mathbb{R}\end{cases}\quad i=1,2,\ldots,ni \tag{15}$$

$$\boldsymbol{H}_{11,i}=\begin{cases}\boldsymbol{BIBC}_{i} & B_{meas,i}\in\mathbb{C}\\ \dfrac{\boldsymbol{BIBC}_{i}^{*}}{2} & B_{meas,i}\in\mathbb{R}\end{cases}\quad i=ni+1,ni+2,\ldots,ni+nb \tag{16}$$

$$\boldsymbol{H}_{11,i}=\begin{cases}\boldsymbol{DLF}_{i} & V_{meas,i}\in\mathbb{C}\\ \dfrac{\boldsymbol{DLF}_{i}^{*}}{2} & V_{meas,i}\in\mathbb{R}\end{cases}\quad i=ni+nb+1,ni+nb+2,\ldots,ni+nb+nv \tag{17}$$

$$\boldsymbol{H}_{12,i}=\begin{cases}\boldsymbol{0} & I_{meas,i}\in\mathbb{C}\\ \dfrac{\boldsymbol{I}_{i}}{2} & I_{meas,i}\in\mathbb{R}\end{cases}\quad i=1,2,\ldots,ni \tag{18}$$

$$\boldsymbol{H}_{12,i}=\begin{cases}\boldsymbol{0} & B_{meas,i}\in\mathbb{C}\\ \dfrac{\boldsymbol{BIBC}_{i}^{*}}{2} & B_{meas,i}\in\mathbb{R}\end{cases}\quad i=ni+1,ni+2,\ldots,ni+nb \tag{19}$$

$$\boldsymbol{H}_{12,i}=\begin{cases}\boldsymbol{0} & V_{meas,i}\in\mathbb{C}\\ \dfrac{\boldsymbol{DLF}_{i}^{*}}{2} & V_{meas,i}\in\mathbb{R}\end{cases}\quad i=ni+nb+1,ni+nb+2,\ldots,ni+nb+nv \tag{20}$$

$$\boldsymbol{H}_{12}=\boldsymbol{H}_{21}^{*} \tag{21}$$

$$\boldsymbol{H}_{22}=\boldsymbol{H}_{11}^{*} \tag{22}$$

where $I_{meas,i}$, $B_{meas,i}$, $V_{meas,i}$ are the measurement current injection of the i^{th} bus, the measurement branch current of the i^{th} branch, and the measurement voltage of the i^{th} bus, respectively. The subscript i refers to the i^{th} row of the corresponding matrix. The algorithm is flexible. And $\boldsymbol{H}$ can be formulated if limited measurements are available in a distribution system. Alternatively, for a well-observed system, $\boldsymbol{H}$ can be

fully ranked. And the full rank is considered when the number of measurements or pseudo points is equal to or greater than the number of buses.

This proposed formulation allows a flexible set of power system measurements such as bus injection currents, branch flows, or bus voltage measurements to be integrated into the ACKF DSE algorithm. Bus injection and branch flow measurements can be incorporated in the form of complex current, current magnitude, or power flow measurements. Bus voltage measurements can be incorporated in the form of complex voltage or voltage magnitude measurements. Pseudo-measurements can also be incorporated with relevant changes to $\boldsymbol{R}$.

IV. Error Covariance and Observability

KFs are well-known to provide useful real-time information on the observability of a system. In applications such as state estimation of the distribution system, it can be challenging to analyze and validate the accuracy of estimation. In a deterministic sense, the observability means that the observation of the output over time provides sufficient information to accurately estimate the state of the system [34]. The estimation accuracy depends on the user requirements and the systems in place that act on the estimation. Determining the observability of the distribution network is not a well researched area.

In the traditional WLS method, when there are sufficient measurements, the whole system can be estimated. This is true when the rank of the measurement matrix is equal to the number of unknown state variables. However, the relationship between numerical observability and topological observability is not obvious [30]. With the KF method, the numerical observability depends on the numerical stability of the KF, which is a well-known problem managed through various methods. As long as the KF is numerically stable, the system is observable and does not rely on the rank of the measurement matrix.

One of the benefits of the KF is the produced error covariance, which can be used to provide the information on the accuracy of estimation, assuming accurate inputs of state and measurement error covariance. The *a posteriori* error variance matrix, given by $\boldsymbol{P}_{k|k}$, is the estimated accuracy of the state estimate as calculated by (11). This can also be defined as $\boldsymbol{P}_{k|k} = E\left[\left(\boldsymbol{x}_k - \hat{\boldsymbol{x}}_k\right)\left(\boldsymbol{x}_k - \hat{\boldsymbol{x}}_k\right)^{\mathrm{T}}\right]$.

In this application, the state represents the complex injection current for each bus node. Based on the direct load flow approach, injection current is linearly related to the change in voltage from the source bus. The error covariance of the state can be used to ascertain the error covariance of the voltage estimation from the relationship with $\boldsymbol{DLF}$ [33].

$$\begin{cases}\Delta \boldsymbol{V} = \boldsymbol{DLF}\cdot\boldsymbol{x} \\ \Delta \hat{\boldsymbol{V}} = \boldsymbol{DLF}\cdot\hat{\boldsymbol{x}}\end{cases} \tag{23}$$

If we consider the error covariance for the change in bus voltage due to the change in bus injection current:

$$\boldsymbol{P}_{voltage,k|k} = E\left[\left(\Delta\boldsymbol{V}_k - \Delta\hat{\boldsymbol{V}}_k\right)\left(\Delta\boldsymbol{V}_k - \Delta\hat{\boldsymbol{V}}_k\right)^{\mathrm{T}}\right] \tag{24}$$

We can substitute (23) into (24) as:

$$\begin{aligned}\boldsymbol{P}_{voltage,k|k} &= E\left[\left(\Delta\boldsymbol{V}_k - \Delta\hat{\boldsymbol{V}}_k\right)\left(\Delta\boldsymbol{V}_k - \Delta\hat{\boldsymbol{V}}_k\right)^{\mathrm{T}}\right] = \\ &E\left[\boldsymbol{DLF}\cdot\left(\boldsymbol{x}-\hat{\boldsymbol{x}}\right)\left(\boldsymbol{x}-\hat{\boldsymbol{x}}\right)^{\mathrm{T}}\cdot\boldsymbol{DLF}^{\mathrm{T}}\right] = \\ &\boldsymbol{DLF}\cdot E\left[\left(\boldsymbol{x}-\hat{\boldsymbol{x}}\right)\left(\boldsymbol{x}-\hat{\boldsymbol{x}}\right)^{\mathrm{T}}\right]\cdot\boldsymbol{DLF}^{\mathrm{T}} = \\ &\boldsymbol{DLF}\cdot\boldsymbol{P}_{k|k}\cdot\boldsymbol{DLF}^{\mathrm{T}}\end{aligned}$$

In augmented complex form, the error covariance for the bus voltages is given by:

$$\boldsymbol{P}_{voltage,k|k} = \boldsymbol{DLF}^{a}\cdot\boldsymbol{P}_{k|k}\cdot\left(\boldsymbol{DLF}^{a}\right)^{\mathrm{T}} \tag{25}$$

where $\boldsymbol{DLF}^{a} = \begin{bmatrix}\boldsymbol{DLF} & \boldsymbol{0} \\ \boldsymbol{0} & \boldsymbol{DLF}^{*}\end{bmatrix}$.

Similarly, the branch error covariance can be derived through the relationship with $\boldsymbol{BIBC}$:

$$\boldsymbol{P}_{branch,k|k} = \boldsymbol{BIBC}^{a}\cdot\boldsymbol{P}_{k|k}\cdot\left(\boldsymbol{BIBC}^{a}\right)^{\mathrm{T}} \tag{26}$$

where $\boldsymbol{BIBC}^{a} = \begin{bmatrix}\boldsymbol{BIBC} & \boldsymbol{0} \\ \boldsymbol{0} & \boldsymbol{BIBC}\end{bmatrix}$.

$\boldsymbol{BIBC}$ is a nonnegative integer matrix, which means that $\boldsymbol{BIBC}^{*} = \boldsymbol{BIBC}$. The error variance is simply the diagonal elements of the error covariance matrix.

At each time step k, the *a posteriori* error variance in augmented complex form is given by:

$$\boldsymbol{P}_{k|k} = \boldsymbol{P}_{k|k-1}\left(\boldsymbol{I} - \boldsymbol{G}_k\boldsymbol{H}_k^{a}\right) \tag{27}$$

where $\boldsymbol{G}_k$ is the optimal Kalman gain, calculated by (9).

The Riccati update equation is derived as $\boldsymbol{P}_{k+1|k} = \boldsymbol{Q}^{a} + \boldsymbol{P}_{k|k-1} - \boldsymbol{P}_{k|k-1}\boldsymbol{H}^{aH}\left(\boldsymbol{H}^{a}\boldsymbol{P}_{k|k-1}\boldsymbol{H}^{aH} + \boldsymbol{R}^{a}\right)^{-1}\boldsymbol{H}^{a}\boldsymbol{P}_{k|k-1}$, where $\boldsymbol{R}^{a}$ is the measurement error covariance matrix.

For simplicity, it is assumed that the measurement matrix, state error covariance matrix, and measurement error covariance matrix do not change per time step. We can calculate the sensitivity of the error covariance to measurement location as:

$$\begin{aligned}\frac{\partial\boldsymbol{P}_{k+1}}{\partial R_i} = \frac{\partial\boldsymbol{P}_k}{\partial R_i} - \boldsymbol{P}_k\boldsymbol{H}^{aH}\left[\boldsymbol{S}\boldsymbol{H}^{a}\frac{\partial\boldsymbol{P}_k}{\partial R_i} - \boldsymbol{S}R_i\boldsymbol{S}\left(\boldsymbol{H}^{a}\boldsymbol{P}_k\right)\right] + \\ \frac{\partial\boldsymbol{P}_k}{\partial R_i}\boldsymbol{H}^{aH}\boldsymbol{S}\left(\boldsymbol{H}^{a}\boldsymbol{P}_k\right)\end{aligned} \tag{28}$$

where R_i is the scalar corresponding to the measurement error variance at location i of the measurement model; and $\boldsymbol{S} = \left(\boldsymbol{R}^{a} + \boldsymbol{H}^{a}\boldsymbol{P}_k\boldsymbol{H}^{aH}\right)^{-1}$. This equation provides the sensitivity of state error covariance for the changes to diagonal elements of $\boldsymbol{R}^{a}$. We can ascertain the impact of changes to measurement nodes on the overall accuracy of the estimation.

This is considered beneficial for large distribution networks, where the optimal locations for measurement nodes are not apparent or intuitive. Considering (25) and (26), the error variance of bus voltage and branch current can be calculated, respectively. Note that the equation assumes the current and previous time steps of $\boldsymbol{P}$ are also dependent on R_i. Appendix B shows the derivation of the equation. This equation can be solved iteratively to calculate the steady-state value.

V. Methodology

The modified IEEE 34-bus and IEEE 123-bus test feeders are used to validate the proposed work. The load for each bus is generated using a complex-valued Wiener process with a stochastic perturbation term consisting of a normal distribution with a nonzero mean. The real and imaginary components are considered as independent Wiener processes. The purpose of the non-zero mean is to reflect the inherent different mean loadings on each bus.

A single simulation set and a full simulation set are considered in the results. The purpose of the single simulation set is to show the time-series performance of the ACKF estimator compared with the actual load flow and the WLS estimator. For each simulation set, a total of 200 time steps is generated. The methodology consists of the following steps:

1) Generate complex-valued current injection for each bus location.

2) Initialize the ACKF state estimator.

3) At each time step, solve the load flow.

4) At each time step, update the ACKF state estimator using the available measurement points.

5) Calculate the estimated state of the network.

6) Compare the ACKF state estimator output with the load flow results to determine the estimation error at each time step.

The full simulation set repeats the simulation set 100 times for statistical relevance. The purpose of the full simulation set is to demonstrate the performance over a statistically relevant sample size for determining the accuracy of estimated error variance. The performance is assessed by using two metrics: mean absolute error (MAE), and the normalized mean error variance (NMEV). MAE is calculated across all the simulations for both bus voltage and branch current magnitude:

$$MAE = \frac{1}{m}\sum_{j=1}^{m}\frac{1}{n}\sum_{i=1}^{n}\left|x_i - \hat{x}_i\right| \tag{29}$$

where n is the number of time steps per simulation; and x_i is the parameters of interest, which is the bus voltage and branch current magnitudes. In the results, the voltage magnitude MAE and branch current magnitude MAE are denoted as *VMMAE* and *BMMAE*, respectively.

Over the full simulation set, the actual error variance of the state estimator is calculated using the NMEV for both bus voltage and branch current magnitudes:

$$\begin{cases} MEV = \dfrac{1}{m}\displaystyle\sum_{j=1}^{m}\frac{1}{n}\sum_{i=1}^{n}\left(e_i - \mu_j\right)^2 \\ NMEV = \dfrac{MEV - \min\left(MEV\right)}{\max\left(MEV\right) - \min\left(MEV\right)} \end{cases} \tag{30}$$

where e_i is the error at the time step i for bus voltage and branch current magnitudes; and μ_j is the average error for the simulation set j, i.e., $\mu_j = \dfrac{1}{n}\displaystyle\sum_{i=1}^{n} e_i$.

NMEV is compared with the calculated error covariance of bus voltage and branch current magnitudes from the KF. The error variances are considered as the diagonal elements of the error covariance matrix.

VI. Test Results and Discussion

A. IEEE 34-bus Test Feeder

A modified version of the IEEE 34-bus test feeder is used to simulate the performance as shown in Fig. 1. The feeder consists of the three-phase main section [35] of the feeder. The consideration of an unbalanced network can be achieved by using an unbalanced direct load flow approach [33]. The number of measurement points is deliberately limited to restrict the observability. The available measurements for the state estimator are bus voltage magnitudes and branch power flow, as they are the most commonly available measurements in distribution networks. Based on the network topology of the test feeder, we consider a voltage magnitude and branch power flow measurement at the start of the feeder and approximately half-way along the feeder (voltage magnitude measurements at bus 8, and branch power flow measurements at branches 1 and 9). Bus 800 is the reference with a value of $1\angle 0°$ p.u..

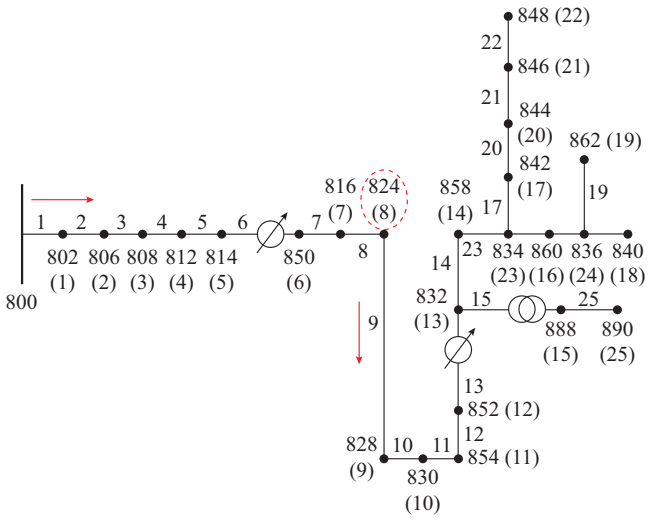

Fig. 1. Modified IEEE 34-bus test feeder.

Based on the formulation in Section III, $\boldsymbol{H}$ is a 3×50 matrix with a rank of 3. Power flow measurements are approximated as complex-valued branch current injections using the voltage of $1\angle 0°$ p.u.. The limited rank $\boldsymbol{H}$ in augmented complex form is:

$$\boldsymbol{H}^a = \begin{bmatrix} \boldsymbol{BIBC}_1 & \boldsymbol{0} \\ \boldsymbol{BIBC}_9 & \boldsymbol{0} \\ \dfrac{\boldsymbol{DLF}_8}{2} & \dfrac{\boldsymbol{DLF}_8^*}{2} \\ \boldsymbol{0} & \boldsymbol{BIBC}_1^* \\ \boldsymbol{0} & \boldsymbol{BIBC}_9^* \\ \dfrac{\boldsymbol{DLF}_8}{2} & \dfrac{\boldsymbol{DLF}_8^*}{2} \end{bmatrix} \tag{31}$$

where $\boldsymbol{BIBC}_i$ and $\boldsymbol{DLF}_i$ are the i^{th} rows of the $\boldsymbol{BIBC}$ and $\boldsymbol{DLF}$ matrices, respectively. The row corresponds to the

branch or bus measurement point. $\boldsymbol{H}$ is formulated using the three measurements available: two branch power flow and one voltage magnitude.

B. Single Simulation Set

Figure 2 shows the comparison of the actual results with the ACKF estimated output for three selected buses. Bus 8 has a voltage magnitude measurement, and buses 15 and 22 are located at the feeder extremities. Figure 3 shows the estimation error for voltage magnitude and voltage angle at each of bus.

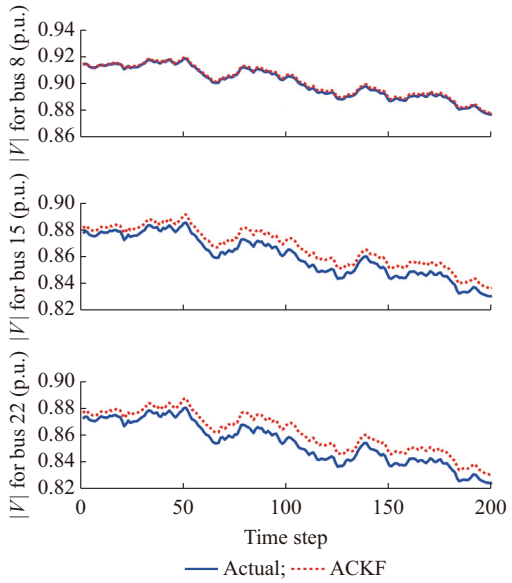

Fig. 2. Comparison of actual results and ACKF method for selected buses.

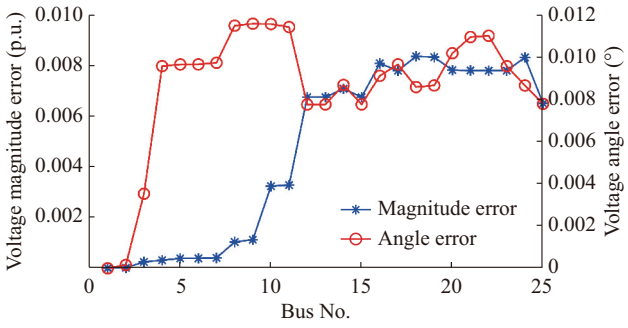

Fig. 3. Voltage magnitude and angle errors for single simulation set.

The results show that the voltage magnitude error worsens the downstream of the voltage magnitude measurement location. However, the results also show a consistent error in the voltage angle estimation, which seems independent of the measurement locations. This is not unreasonable since the only corrective information for voltage angle is the single branch power flow measurement at branch 9.

Figure 4 shows the comparison of active and reactive power flows for branches 1, 5, 9, and 18. Although branch 9 has a power flow measurement, there is an error associated due to the approximation of branch current from power flow measurements. There is a progressive increase in error because of the limited information available.

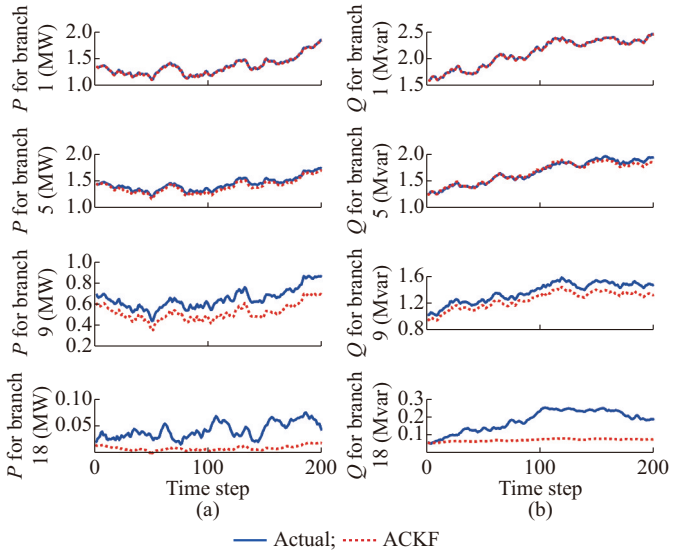

Fig. 4. Comparison of actual results and ACKF method on active and reactive power flows for selected branches. (a) Active power flow. (b) Reactive power flow.

The ACKF method is also compared with the traditional WLS and iterated extended KF (IEKF) formulation to demonstrate the improved performance. For each bus, the comparison for voltage magnitude and voltage angle errors is shown in Fig. 5.

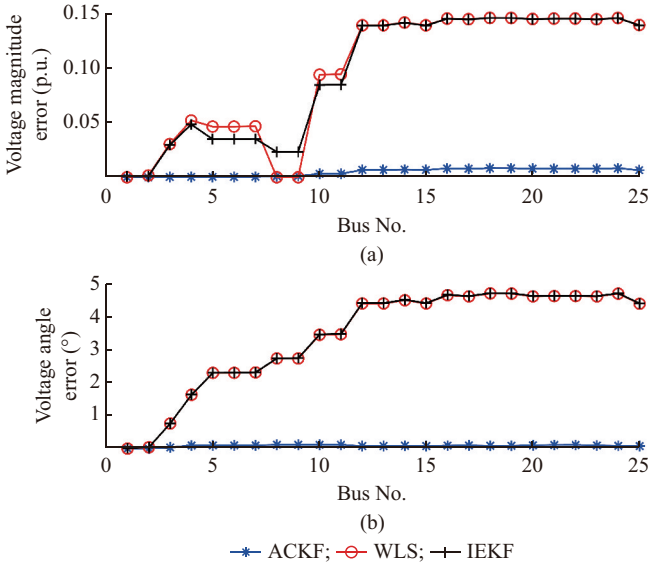

Fig. 5. Comparison of voltage magnitude and voltage angle errors among ACKF, WLS and IEKF methods. (a) Voltage magnitude error. (b) Voltage angle error.

The three methods are calculated using the same parameters such as measurement data, error covariances, and convergence tolerances, to ensure consistent comparisons. Both WLS and IEKF methods converge to similar steady-state values, which is not unexpected since the IEKF method is based on similar nonlinear measurement models of WLS estimators. The IEKF method uses a recursive algorithm to predict the state based on a linearization using the Jacobian,

and a corrective step based on the Kalman gain. Like the WLS method, the IEKF method is an iterative process that terminates when the output converges to a defined tolerance threshold.

The ACKF method demonstrates the improved accuracy over both WLS and IEKF methods. The deficiencies of the traditional WLS method are well-known, particularly in situations with limited measurement data [30]. This is also the case with KF methods that are built off the same foundation as WLS methods.

C. Full Simulation Set

The NMEV for bus voltage and branch current magnitudes is shown in Fig. 6 and Fig. 7, respectively. The error variance is calculated based on the KF error covariance, as per (25) and (26), and compared with the actual error variance from the simulations. The error variance of the KF is closely correlated with the actual error variance over the full set of time-series simulations with randomly generated bus injection current.

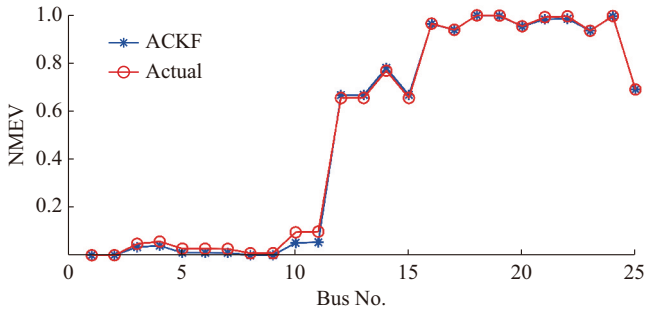

Fig. 6. NMEV for bus voltage magnitude.

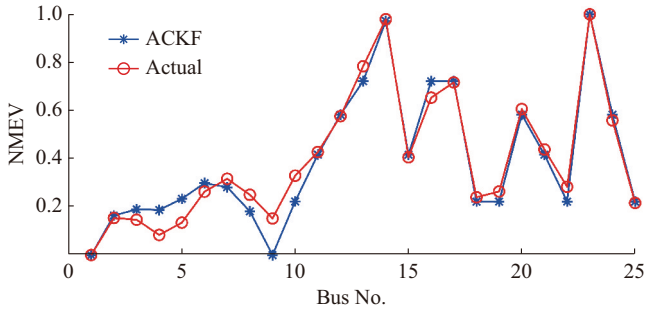

Fig. 7. NMEV for branch current magnitude.

In practical terms, this means it would be possible to accurately infer the estimation error variance for bus voltage and branch current magnitudes through the ACKF process.

D. Computation Efficiency

The computation time for ACKF, WLS, and IEKF methods is shown in Table I. The simulations are conducted on a PC with an Intel Core i7-4770 3.4 GHz processor and 16 GB of RAM. The ACKF and WLS methods are calculated by using the same initial conditions and parameters over the full simulation set. The average computation time is taken for each simulation set, and the minimum, maximum, and mean of the full simulation sets are calculated. The results show that ACKF has a consistently better computation performance compared with the WLS and IEKF methods. It is also found that IEKF has a heavier computation compared with WLS, which is consistent with the previous research [36].

TABLE I
COMPUTATION TIMES OVER FULL SIMULATION SET

Extent	Computation time (ms)		
	ACKF	WLS	IEKF
Minimum	18	40	42
Mean	20	44	72
Maximum	72	47	64

E. Sensitivity of Error Variance to Measurements

The previous results show that the ACKF process could accurately estimate the error variance of voltage and branch current magnitudes. We can determine the optimal locations for additional measurements by calculating the predicted sensitivity $\partial \boldsymbol{P}_{k+1|k}/\partial R_{ii}$ from (28). This equation yields the sensitivity of the estimated state error covariance matrix $\boldsymbol{P}$ to changes in $\boldsymbol{R}$. These changes can be used to improve an existing measurement point or considering an entirely new measurement in the system.

In the previous section, the limited rank $\boldsymbol{H}$ is formulated as per (31), which only consists of three measurement points. We can use a full ranked $\boldsymbol{H}$ to calculate the sensitivity of the error variance for every bus voltage magnitude or branch current magnitude. For example, if a new voltage magnitude measurement is installed at bus 20, what is the change in error variance across all the bus voltage or branch current magnitudes?

Figure 8 shows the sensitivity of voltage magnitude error variance at bus nodes to the changes of voltage measurement locations, which shows a high sensitivity to bus voltage measurements downstream of bus 9.

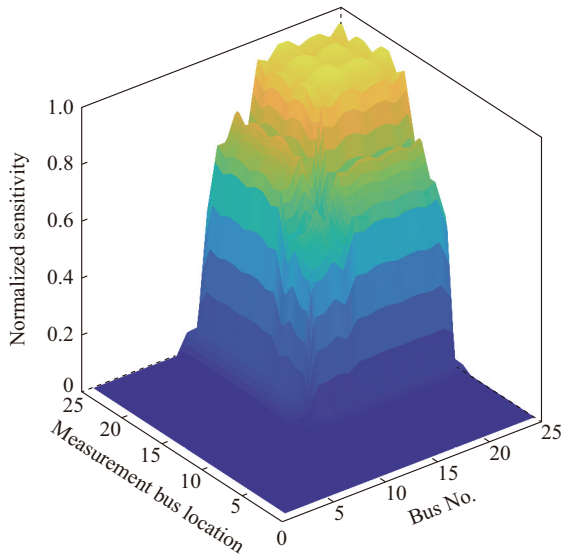

Fig. 8. Sensitivity of voltage magnitude error variance to voltage magnitude measurements.

The installation of voltage measurement sensors upstream of bus 9 is not recommended since error variance will not be improved. Similarly, Fig. 9 shows the effects of additional voltage magnitude measurements on branch current magnitude error variance. This shows that the optimal location of an additional voltage magnitude measurement will be around bus 12, which has the highest sensitivity in error variance for both bus voltage and branch current magnitudes. Figure 10 shows the corresponding changes in voltage magnitude and branch magnitude MAE for an additional voltage measurement on bus 12.

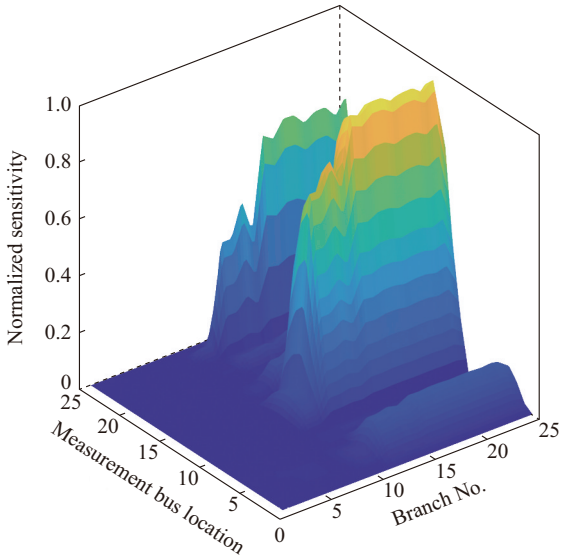

Fig. 9. Sensitivity of branch current magnitude error variance to voltage magnitude measurements.

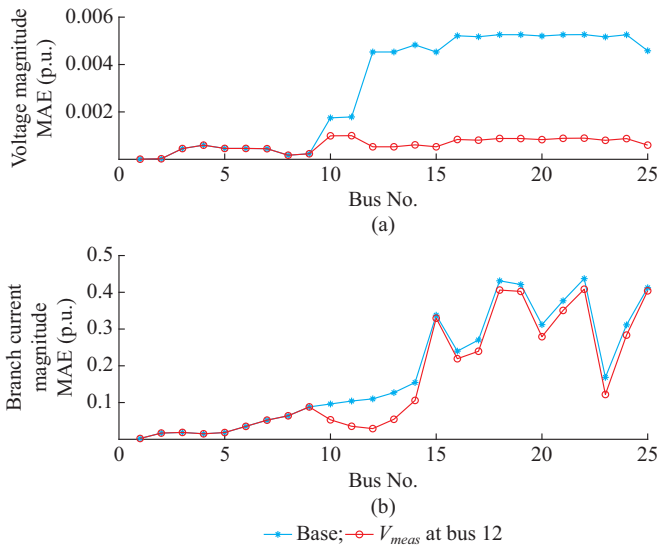

Fig. 10. Changes in voltage current and branch magnitude error from additional voltage magnitude measurement at bus 12. (a) Voltage magnitude MAE. (b) Branch current magnitude MAE.

F. IEEE 123-bus Test Feeder

The proposed method is tested on a modified IEEE 123-bus test feeder to demonstrate the scalability of the algorithm. Like the IEEE 34-bus test case, the feeder only includes positive sequence network. The consideration of a three-phase unbalanced network can be achieved using the unbalanced direct load flow method [33]. The load data is generated using a complex-valued Wiener Process and run over 100 simulation sets, each set with 200 time steps. The number of measurements is limited to 10-bus voltage magnitude and ten branch power flow, with the locations shown in Fig. 11. Note that the bus voltage and branch power flow are considered as separate and independent measurements and do not consider that power flow measurements would also include a voltage and a current measurement. The measurement points are scattered to provide the visibility across the network at approximate key locations.

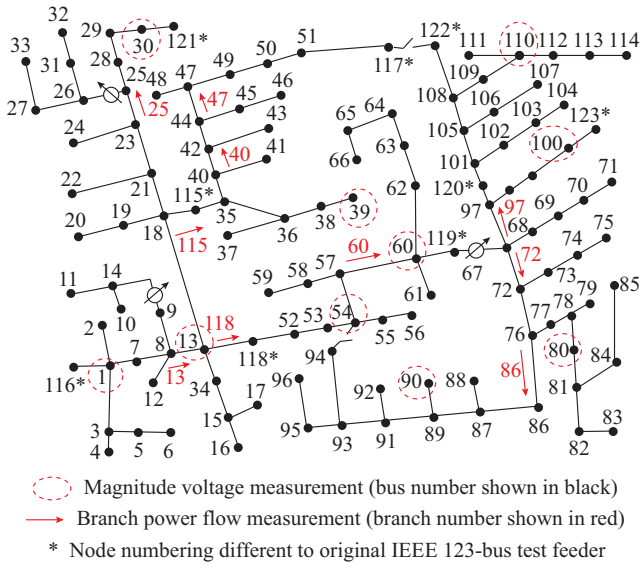

Fig. 11. Modified IEEE 123-bus test feeder.

The average error in voltage magnitude and voltage angle across the full simulation set is shown in Fig. 12. The results show a higher error at the extremities of the feeder. Buses 66, 104 and 107 are the highest because there are limited measurement points compared with other parts of the feeder.

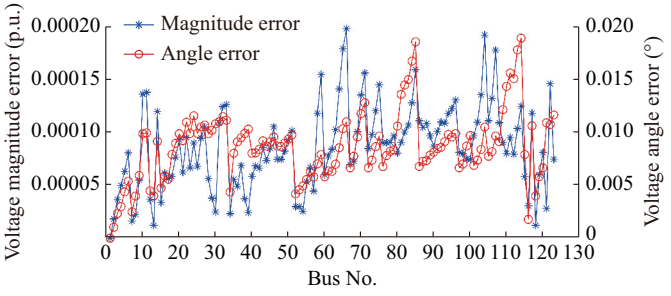

Fig. 12. Average voltage magnitude and voltage angle errors across all simulation sets.

The NMEV of bus voltage and branch current magnitudes is shown in Figs. 13 and 14, respectively. There is a strong correlation between the ACKF predicted error variance and

actual error variance for voltage magnitude. This allows easy identification of buses that may have high error variance in the estimation output. There is a good correlation in the predicted branch current error variance compared with the actual one. However, there are some discrepancies. Firstly, branch power flow measurements are not ideal for the ACKF estimator since it relies on a linear calculation of network state. The algorithm implements an assumption to convert branch power flow to current and uses an angle compensation to correct the measurement model. Branch or injection current measurements are preferred. Secondly, the number of available measurement points is limited, which affects the observability of the estimator. In general, the ACKF estimator can reasonably predict the error variance of the branch current magnitude estimate.

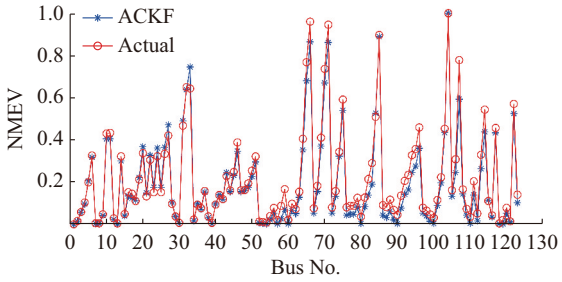

Fig. 13. NMEV of bus voltage magnitude for IEEE 123-bus test feeder.

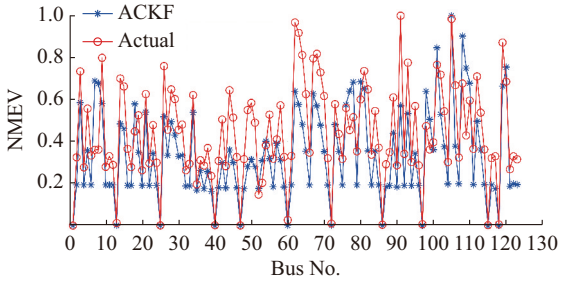

Fig. 14. NMEV of branch current magnitude for IEEE 123-bus test feeder.

VII. Conclusion

This paper demonstrates an alternative approach to DSE based on ACKF and provides a generalized formulation of the ACKF DSE to allow various types of measurements to be incorporated into a complex-valued estimator. The results demonstrate an improved performance of ACKF compared with the traditional WLS method, particularly with limited measurement points. The simulation results also demonstrate the ability of ACKF method to provide an accurate estimation of error variance of bus voltage and branch current magnitudes based on randomly generated Wiener process complex-valued load data. In practical terms, this capability provides vital information for systems relying on DSE, as the error variance can be accurately estimated. The proposed sensitivity of error variance also allows operators to determine optimal locations for additional measurements by showing the changes in error variance across all bus and branch locations in a simple offline calculation.

Appendix A

$$\boldsymbol{H}=\begin{bmatrix}\boldsymbol{I}_{ni\times m}\\ \boldsymbol{BIBC}_{nb\times m}\\ -\boldsymbol{DLF}_{nv\times m}\end{bmatrix} \tag{A1}$$

$$\boldsymbol{H}^{a}=\begin{bmatrix}\boldsymbol{I}_{ni\times m} & \boldsymbol{0}_{ni\times m}\\ \boldsymbol{BIBC}_{nb\times m} & \boldsymbol{0}_{nb\times m}\\ -\boldsymbol{DLF}_{nv\times m} & \boldsymbol{0}_{nv\times m}\\ \boldsymbol{0}_{ni\times m} & \boldsymbol{I}_{ni\times m}\\ \boldsymbol{0}_{nb\times m} & \boldsymbol{BIBC}^{*}_{nb\times m}\\ \boldsymbol{0}_{nv\times m} & -\boldsymbol{DLF}^{*}_{nv\times m}\end{bmatrix} \tag{A2}$$

where ni is the number of bus injection current measurements; nb is the number of branch current measurements; and nv is the number of bus voltage measurements.

Appendix B

The following shows the derivation of the sensitivity of the error covariance to the diagonal of R_i.

$$\boldsymbol{P}_{k+1|k}=\boldsymbol{Q}^{a}+\boldsymbol{P}_{k|k-1}-\boldsymbol{P}_{k|k-1}\boldsymbol{H}^{aH}\left(\boldsymbol{H}^{a}\boldsymbol{P}_{k|k-1}\boldsymbol{H}^{aH}+\boldsymbol{R}^{a}\right)^{-1}\boldsymbol{H}^{a}\boldsymbol{P}_{k|k-1} \tag{B1}$$

$$\frac{\partial\boldsymbol{P}_{k+1|k}}{\partial R_i}=\frac{\partial\boldsymbol{P}_{k|k-1}}{\partial R_i}-\frac{\partial}{\partial R_i}\left[\boldsymbol{P}_{k|k-1}\boldsymbol{H}^{aH}\left(\boldsymbol{H}^{a}\boldsymbol{P}_{k|k-1}\boldsymbol{H}^{aH}+\boldsymbol{R}^{a}\right)^{-1}\boldsymbol{H}^{a}\boldsymbol{P}_{k|k-1}\right] \tag{B2}$$

$\boldsymbol{A}$, $\boldsymbol{B}$, and $\boldsymbol{C}$ are defined as follows:

$$\begin{cases}\boldsymbol{A}=\boldsymbol{P}_{k|k-1}\boldsymbol{H}^{aH}\\ \boldsymbol{B}=\left(\boldsymbol{R}^{a}+\boldsymbol{H}^{a}\boldsymbol{P}_{k|k-1}\boldsymbol{H}^{aH}\right)^{-1}\\ \boldsymbol{C}=\boldsymbol{H}^{a}\boldsymbol{P}_{k|k-1}\end{cases} \tag{B3}$$

Consider the following matrix derivative identities:

$$\begin{cases}\dfrac{\partial(\boldsymbol{ABC})}{\partial\boldsymbol{x}}=\boldsymbol{A}\dfrac{\partial(\boldsymbol{BC})}{\partial\boldsymbol{x}}+\dfrac{\partial\boldsymbol{A}}{\partial\boldsymbol{x}}(\boldsymbol{BC})\\ \qquad\qquad=\boldsymbol{A}\left(\boldsymbol{B}\dfrac{\partial\boldsymbol{C}}{\partial\boldsymbol{x}}+\dfrac{\partial\boldsymbol{B}}{\partial\boldsymbol{x}}\boldsymbol{C}\right)+\dfrac{\partial\boldsymbol{A}}{\partial\boldsymbol{x}}(\boldsymbol{BC})\\ \dfrac{\partial\boldsymbol{D}^{-1}}{\partial\boldsymbol{x}}=-\boldsymbol{D}^{-1}\dfrac{\partial\boldsymbol{D}}{\partial\boldsymbol{x}}\boldsymbol{D}^{-1}\end{cases} \tag{B4}$$

Therefore, we can obtain:

$$\begin{cases}\dfrac{\partial\boldsymbol{A}}{\partial R_i}=\dfrac{\partial\boldsymbol{P}_{k|k-1}}{\partial R_i}\boldsymbol{H}^{aH}\\ \dfrac{\partial\boldsymbol{B}}{\partial R_i}=-\left(\boldsymbol{R}^{a}+\boldsymbol{H}^{a}\boldsymbol{P}_{k}\boldsymbol{H}^{aH}\right)^{-1}R_{ii}\left(\boldsymbol{R}^{a}+\boldsymbol{H}^{a}\boldsymbol{P}_{k}\boldsymbol{H}^{aH}\right)^{-1}\\ \dfrac{\partial\boldsymbol{C}}{\partial R_i}=\boldsymbol{H}^{a}\dfrac{\partial\boldsymbol{P}_{k|k-1}}{\partial R_i}\end{cases} \tag{B5}$$

If we consider (B3), (B4), and (B5), (B2) can be re-written as:

$$\frac{\partial\boldsymbol{P}_{k+1}}{\partial R_i}=\frac{\partial\boldsymbol{P}_{k}}{\partial R_i}-\boldsymbol{P}_{k}\boldsymbol{H}^{aH}\left[\boldsymbol{S}\boldsymbol{H}^{a}\frac{\partial\boldsymbol{P}_{k}}{\partial R_i}+\frac{\partial\boldsymbol{S}}{\partial R_i}\left(\boldsymbol{H}^{a}\boldsymbol{P}_{k}\right)\right]+\frac{\partial\boldsymbol{P}_{k}}{\partial R_i}\boldsymbol{H}^{aH}\boldsymbol{S}\left(\boldsymbol{H}^{a}\boldsymbol{P}_{k}\right) \tag{B6}$$

$$\boldsymbol{S}=\left(\boldsymbol{R}^{a}+\boldsymbol{H}^{a}\boldsymbol{P}_{k}\boldsymbol{H}^{aH}\right)^{-1} \tag{B7}$$

REFERENCES

[1] F. C. Schweppe and E. J. Handschin, "Static state estimation in electric power systems," *Proceedings of IEEE*, vol. 62, no. 7, pp. 972-982, Jan. 1974.

[2] F. C. Schweppe and J. Wildes, "Power system static-state estimation, part I: exact model," *IEEE Transactions on Power Apparatus and Systems*, vol. PAS-89, no. 1, pp. 120-125, Jan. 1970.

[3] F. C. Schweppe and D. B. Rom, "Power system static-state estimation, part II: approximate model," *IEEE Transactions on Power Apparatus and Systems*, vol. PAS-89, no. 1, pp. 125-130, Jan. 1970.

[4] F. C. Schweppe, "Power system static-state estimation, part III: implementation," *IEEE Transactions on Power Apparatus and Systems*, vol. PAS-89, no. 1, pp. 130-135, Jan. 1970.

[5] A. Monticelli, "Electric power system state estimation," *Proceedings of IEEE*, vol. 88, no. 2, pp. 262-282, Feb. 2000.

[6] W. Zheng, W. Wu, A. Gomez-Exposito *et al*., "Distributed robust bilinear state estimation for power systems with nonlinear measurements," *IEEE Transactions on Power Systems*, vol. 32, no. 1, pp. 499-509, Jan. 2017.

[7] J. Zhao, L. Mili, and R. C. Pires, "Statistical and numerical robust state estimator for heavily loaded power systems," *IEEE Transactions on Power Systems*, vol. 33, no. 6, pp. 6904-6914, Nov. 2018.

[8] W. Zheng, W. Wu, X. Shi *et al*., "A robust bilinear three-phase state estimation method for power systems," in *Proceedings of 2016 IEEE PES General Meeting*, Boston, USA, Jul. 2016, pp. 1-4.

[9] C. H. Ho, H. C. Wu, S. C. Chan *et al*., "A robust statistical approach to distributed power system state estimation with bad data," *IEEE Transactions on Smart Grid*, vol. 11, no. 1, pp. 517-527, Jan. 2020.

[10] M. B. D. C. Filho and J. C. S. de Souza, "Forecasting-aided state estimation – part I: panorama," *IEEE Transactions on Power Systems*, vol. 24, no. 4, pp. 1667-1677, Nov. 2009.

[11] M. B. D. C. Filho, J. C. S. de Souza, and R. S. Freund, "Forecasting-aided state estimation – part II: implementation," *IEEE Transactions on Power Systems*, vol. 24, no. 4, pp. 1678-1685, Nov. 2009.

[12] J. Zhao, A. Gómez-Expósito, M. Netto *et al.*, "Power system dynamic state estimation: motivations, definitions, methodologies, and future work," *IEEE Transactions on Power Systems*, vol. 34, no. 4, pp. 3188-3198, Jul. 2019.

[13] A. Paul, I. Kamwa, and G. Joos, "Centralized dynamic state estimation using a federation of extended Kalman filters with intermittent PMU data from generator terminals," *IEEE Transactions on Power Systems*, vol. 33, no. 6, pp. 6109-6119, Nov. 2018.

[14] S. Kanna, D. H. Dini, Y. Xia *et al.*, "Distributed widely linear Kalman filtering for frequency estimation in power networks," *IEEE Transactions on Signal and Information Processing over Networks*, vol. 1, no. 1, pp. 45-57, Mar. 2015.

[15] E. Ghahremani and I. Kamwa, "Dynamic state estimation in power system by applying the extended Kalman filter with unknown inputs to phasor measurements," *IEEE Transactions on Power Systems*, vol. 26, no. 4, pp. 2556-2566, Nov. 2011.

[16] E. A. Blood, M. D. Ilic, J. Ilic *et al.*, "A Kalman filter approach to quasi-static state estimation in electric power systems," in *Proceedings of 2006 38th North American Power Symposium*, Carbondale, USA, Sept. 2006, pp. 417-422.

[17] E. A. Blood, B. H. Krogh, and M. D. Ilic, "Electric power system static state estimation through Kalman filtering and load forecasting," in *Proceedings of 2008 IEEE PES General Meeting*, Pittsburgh, USA, Jul. 2008, pp. 1-6.

[18] R. Gelagaev, P. Vermeyen, and J. Driesen, "State estimation in distribution grids," in *Proceedings of 2008 13th International Conference on Harmonics and Quality of Power*, Wollongong, Australia, Sept. 2008, pp. 1-6.

[19] L. Hu, Z. Wang, I. Rahman *et al*., "A constrained optimization approach to dynamic state estimation for power systems including PMU and missing measurements," *IEEE Transactions on Control Systems Technology*, vol. 24, no. 2, pp. 703-710, Mar. 2016.

[20] S. Sarri, M. Paolone, R. Cherkaoui *et al.*, "State estimation of active distribution networks: comparison between WLS and iterated Kalman-filter algorithm integrating PMUs," in *Proceedings of 2012 3rd IEEE PES Innovative Smart Grid Technologies Europe (ISGT Europe)*, Berlin, Germany, Oct. 2012, pp. 1-8.

[21] G. Valverde and V. Terzija, "Unscented Kalman filter for power system dynamic state estimation," *IET Generation, Transmission & Distribution*, vol. 5, no. 1, pp. 29-37, Jan. 2011.

[22] J. Zhao and L. Mili, "Robust unscented Kalman filter for power system dynamic state estimation with unknown noise statistics," *IEEE Transactions on Smart Grid*, vol. 10, no. 2, pp. 1215-1224, Mar. 2019.

[23] E. Ghahremani and I. Kamwa, "Local and wide-area PMU-based decentralized dynamic state estimation in multi-machine power systems," *IEEE Transactions on Power Systems*, vol. 31, no. 1, pp. 547-562, Jan. 2016.

[24] W. S. Rosenthal, A. M. Tartakovsky, and Z. Huang, "Ensemble Kalman filter for dynamic state estimation of power grids stochastically driven by time-correlated mechanical input power," *IEEE Transactions on Power Systems*, vol. 33, no. 4, pp. 3701-3710, Jul. 2018.

[25] B. Uzunoğlu and M. A. Ülker, "Maximum likelihood ensemble filter state estimation for power systems," *IEEE Transactions on Instrumemt Measurement*, vol. 67, no. 9, pp. 2097-2106, Sept. 2018.

[26] M. Shafiei, "Distribution network state estimation, time dependency and fault detection," Ph. D. dissertation, Queensland University of Technology, Brisbane, Australia, 2019.

[27] S. L. Goh and D. P. Mandic, "An augmented extended Kalman filter algorithm for complex-valued recurrent neural networks," in *Proceedings of 2006 IEEE International Conference on Acoustics Speed and Signal Processing Proceedings*, Toulouse, France, May 2006, pp. 1-5.

[28] A. Arefi, G. Ledwich, and B. Behi, "An efficient DSE using conditional multivariate complex gaussian distribution," *IEEE Transactions on Smart Grid*, vol. 6, no. 4, pp. 2147-2156, Jul. 2015.

[29] M. Shafiei, A. Arefi, G. Nourbakhsh *et al.*, "Spatial-temporal state estimation using CMCGD applied to distribution networks," in *Proceedings of 2017 IEEE PES Innovative Smart Grid Technologies Conference Europe (ISGT-Europe)*, Torino, Italy, Sept. 2017, pp. 1-6.

[30] C. Lu, J. Teng, and W. Liu, "Distribution system state estimation," *IEEE Transactions on Power Systems*, vol. 10, no. 1, pp. 229-240, Jan. 1995.

[31] C. Chong and A. Debs, "Statistical synthesis of power system functional load models," in *Proceedings of 1979 18th IEEE Conference on Decision and Control including the Symposium on Adaptive Processes*, Fort Lauderdale, USA, Dec. 1979, pp. 264-269.

[32] Y. Qiu, J. Zhao, and H. Chiang, "Effects of the stochastic load model on power system voltage stability based on bifurcation theory," in *Proceedings of 2008 IEEE/PES Transmission and Distribution Conference and Exposition*, Chicago, USA, Apr. 2008, pp. 1-6.

[33] J. Teng, "A direct approach for distribution system load flow solutions," *IEEE Transactions on Power Delivery*, vol. 18, no. 3, pp. 882-887, Jul. 2003.

[34] F. Ham and R. Brown, "Observability, eigenvalues, and Kalman filtering," *IEEE Transactions on Aerospace and Electronic Systems*, vol. AES-19, no. 2, pp. 269-273, Mar. 1983.

[35] N. Mwakabuta and A. Sekar, "Comparative study of the IEEE 34 node test feeder under practical simplifications," in *Proceedings of 2007 39th North American Power Symposium*, Las Cruces, USA, Sept. 2007, pp. 484-491.

[36] A. Alamin, H. M. Khalid, and J. Peng, "Power system state estimation based on iterative extended Kalman filtering and bad data detection using normalized residual test," in *Proceedings of 2015 IEEE Power and Energy Conference at Illinois (PECI)*, Champaign, USA, Feb. 2015, pp. 1-5.

Alan Louis received a B.Eng (Hons) degree from James Cook University, Townsville, Australia, in 2008 and is currently pursuing a Ph.D. degree with the Queensland University of Technology, Brisbane, Australia. He is a registered professional engineer in Queensland, Australia with over 10 years experience in the power industry. He is currently working as a principal engineer for Energy Queensland, an Australian distribution network service provider. His research interests include control systems, distributed energy resource integration, large renewable connections and power system modelling.

Gerard Ledwich received the Ph.D. degree in electrical engineering from the University of Newcastle, Newcastle, Australia, in 1976. He is a Chair Professor in electrical asset management with the School of Electrical Engineering and Computer Science, Queensland University of Technology, Brisbane, Australia. His research interests include power systems, power electronics, and wide area control of smart grid.

Geoffrey Walker received the B.E. and Ph.D. degrees from the University of Queensland (UQ), Brisbane, Australia, in 1990 and 1999, respectively. From 1998 to 2007, he was the Power Electronics Lecturer with UQ. From

2008 to 2013, he was a Senior Electrical Engineering Consultant with Aurecon's Transmission and Distribution Group, Brisbane, Australia, across various areas including rail traction, grounding studies, electricity transmission planning, and renewable energy project design, and review. In 2013, he joined the Electrical Power Engineering Group, Queensland University of Technology, Brisbane, Australia, as an Associate Professor. His current research interests include applying power electronics to applications in renewable energy (especially photovoltaic), power systems, and electric vehicles.

Yateendra Mishra received the Ph. D. degree from the University of Queensland, Brisbane, Australia, in 2009. He is currently a Senior Lecturer and Advanced Queensland Research Fellow with the School of Electrical Engineering and Computer Science, Queensland University of Technology, Brisbane, Australia. His research interests include distributed generation, distributed energy storage, power system stability and control, and their applications in smart grid.